

UNCLASSIFIED

AD NUMBER
ADB216947
NEW LIMITATION CHANGE
TO Approved for public release, distribution unlimited
FROM Distribution authorized to U.S. Gov't. agencies only; Proprietary Info.; Oct 96. Other requests shall be referred to Commander, Army Medical Research and Materiel Command, Attn: MCMR-RMI-S, Fort Detrick, Frederick, MD 21702-5012.
AUTHORITY
USAMRMC ltr, 4 Dec 2002

THIS PAGE IS UNCLASSIFIED

AD \_\_\_\_\_

CONTRACT NUMBER DAMD17-96-C-6050

TITLE: Low-Power, Non-Invasive Physiological Sensors for Remote Usage

PRINCIPAL INVESTIGATOR: Dr. Tapesb Yadav

CONTRACTING ORGANIZATION: Nanomaterials Research Corporation  
Tucson, AZ 85706

REPORT DATE: October 1996

TYPE OF REPORT: Final-Phase I

PREPARED FOR: Commander  
U.S. Army Medical Research and Materiel Command  
Fort Detrick, Frederick, Maryland 21702-5012

DISTRIBUTION STATEMENT: Distribution authorized to U.S. Government agencies only (proprietary information, Oct 96). Other requests for this document shall be referred to Commander, U.S. Army Medical Research and Materiel Command, ATTN: MCMR-RMI-S, Fort Detrick, Frederick, MD 21702-5012.

The views, opinions and/or findings contained in this report are those of the author(s) and should not be construed as an official Department of the Army position, policy or decision unless so designated by other documentation.

19961209 064

# REPORT DOCUMENTATION PAGE

Form Approved  
OMB No. 0704-0188

Public reporting burden for this collection of information is estimated to average 1 hour per response, including the time for reviewing instructions, searching existing data sources, gathering and maintaining the data needed, and completing and reviewing the collection of information. Send comments regarding this burden estimate or any other aspect of this collection of information, including suggestions for reducing this burden, to Washington Headquarters Services, Directorate for Information Operations and Reports, 1215 Jefferson Davis Highway, Suite 1204, Arlington, VA 22202-4302, and to the Office of Management and Budget, Paperwork Reduction Project (0704-0188), Washington, DC 20503.

<b>1. AGENCY USE ONLY (Leave blank)</b>		<b>2. REPORT DATE</b> October 1996	<b>3. REPORT TYPE AND DATES COVERED</b> Final-Phase 1 (30 Mar 96 - 29 Sep 96)	
<b>4. TITLE AND SUBTITLE</b> Low-Power, Non-Invasive Physiological Sensors for Remote Usage			<b>5. FUNDING NUMBERS</b> DAMD17-96-C-6050	
<b>6. AUTHOR(S)</b> Dr. Tapesb Yadav				
<b>7. PERFORMING ORGANIZATION NAME(S) AND ADDRESS(ES)</b> Nanomaterials Research Corporation Tucson, AZ 85706			<b>8. PERFORMING ORGANIZATION REPORT NUMBER</b>	
<b>9. SPONSORING/MONITORING AGENCY NAME(S) AND ADDRESS(ES)</b> Commander U.S. Army Medical Research and Materiel Command Fort Detrick, Frederick, Maryland 21702-5012			<b>10. SPONSORING/MONITORING AGENCY REPORT NUMBER</b>	
<b>11. SUPPLEMENTARY NOTES</b>				
<b>12a. DISTRIBUTION / AVAILABILITY STATEMENT</b> Distribution authorized to U.S. Government agencies only (proprietary information, Oct 96). Other requests for this document shall be referred to Commander, U.S. Army Medical Research and Materiel Command, ATTN: MCMR-RMI-S, Fort Detrick, Frederick, Maryland 21702-5012.			<b>12b. DISTRIBUTION CODE</b>	
<b>13. ABSTRACT (Maximum 200)</b>  Oxygen sensors based on oxygen-conducting ceramics have the advantage of simplicity in construction and operation. However, currently available oxygen sensors of this kind require too high temperatures (above 600 °C) to operate. During Phase I, Nanomaterials Research Corporation (NRC) aimed to established the proof-of-concept for developing low-temperature, low power consuming, miniaturized oxygen sensors based on YSB materials. The objectives of the Phase I work included fabricating an oxygen sensor based on YSB nanomaterials, characterizing the sensor components (the electrolyte and the electrodes), testing the sensor, and developing the conceptual basis for a systematic development and optimization work during Phase II. During Phase I, we have studied basic dependence of properties on material, processing, and microstructure of the sensor components, and have identified electrode kinetics as a major performance-limiting factor. Then we have focused on significantly improving the sensor performance by introducing nanostructured composite electrodes. The nanostructured sensors have been evaluated extensively. Phase I results suggest that NRC's nanostructured sensors outperform the base line sensors, and that nanostructured materials are excellent foundation for electrode and electrolyte processing for the sensor applications.				
<b>14. SUBJECT TERMS</b> Oxygen Sensors, Solid State, Nanomaterials			<b>15. NUMBER OF PAGES</b> 25	
			<b>16. PRICE CODE</b>	
<b>17. SECURITY CLASSIFICATION OF REPORT</b> Unclassified	<b>18. SECURITY CLASSIFICATION OF THIS PAGE</b> Unclassified	<b>19. SECURITY CLASSIFICATION OF ABSTRACT</b> Unclassified	<b>20. LIMITATION OF ABSTRACT</b> Limited	

## FOREWORD

Opinions, interpretations, conclusions and recommendations are those of the author and are not necessarily endorsed by the U.S. Army.

✓ Where copyrighted material is quoted, permission has been obtained to use such material.

✓ Where material from documents designated for limited distribution is quoted, permission has been obtained to use the material.

✓ Citations of commercial organizations and trade names in this report do not constitute an official Department of Army endorsement or approval of the products or services of these organizations.

\_\_\_ In conducting research using animals, the investigator(s) adhered to the "Guide for the Care and Use of Laboratory Animals," prepared by the Committee on Care and use of Laboratory Animals of the Institute of Laboratory Resources, national Research Council (NIH Publication No. 86-23, Revised 1985).

\_\_\_ For the protection of human subjects, the investigator(s) adhered to policies of applicable Federal Law 45 CFR 46.

\_\_\_ In conducting research utilizing recombinant DNA technology, the investigator(s) adhered to current guidelines promulgated by the National Institutes of Health.

\_\_\_ In the conduct of research utilizing recombinant DNA, the investigator(s) adhered to the NIH Guidelines for Research Involving Recombinant DNA Molecules.

\_\_\_ In the conduct of research involving hazardous organisms, the investigator(s) adhered to the CDC-NIH Guide for Biosafety in Microbiological and Biomedical Laboratories.

  
\_\_\_\_\_  
PI - Signature

10/25/96  
\_\_\_\_\_  
Date

TABLE OF CONTENT

1. Introduction ..... 5

2. Work done for the Phase I program ..... 6

    2.1. Synthesis of nanosized YSB powder ..... 6

    2.2. Processing of YSB electrolytes ..... 9

    2.3. Electrochemical characterization of conventional Ag|YSB|Ag cells ..... 10

    2.4. Modification of Ag-based electrodes ..... 13

    2.5. Characterization of YSB electrolytes made from YSB nanopowder ..... 17

    2.6. Construction of the sensor testing system ..... 20

    2.7. Evaluation of sensor performance ..... 22

3. Conclusions ..... 24

4. References ..... 24

## 1. INTRODUCTION

Existing equipment for gas exchange-based health monitoring measure many physical parameters. Example parameters include airway pressure, tidal volume, minute volume, temperature, humidity, oxygen concentration in inhaled gases, oxygen and carbon dioxide concentration in exhaled gases, and volatile halogenated hydrocarbons in an anesthetized patient's exhaled breath. One of the problem with existing equipment technology is that the gas sensing step is performed by very bulky and energy intensive techniques (e.g. CO<sub>2</sub> concentration is measured using CO<sub>2</sub> absorber). For remote settings such as combat situations, the bulky and energy intensive equipment can be as debilitating as the potential injury itself. Thus, there is a need for innovations that can help lower the bulk and the energy needs of non-invasive gas exchange monitoring systems.

Oxygen sensors based on oxygen-conducting ceramics, with their simplicity in construction and operation, offer a possible solution to this problem. However, currently available oxygen sensors of this kind, such as yttria-stabilized zirconia (YSZ) oxygen sensors, require too high temperatures to operate. They become inefficient or ineffective if the sensor temperature falls below 600 °C. This problem is again a significant issue because energy is a premium commodity in military applications.

Nanomaterials Research Corporation (NRC), during this program, seeks to develop low temperature, low power consuming, miniaturized oxygen sensors for non-invasive gas exchange monitoring systems. We choose yttria-stabilized bismuth oxide (YSB) as the electrolyte material, because YSB has higher conductivity than YSZ at temperatures below 700 °C. With this material it is possible to make oxygen sensors with an operation temperature lower or much lower than that for YSZ based sensors (e.g. below 500 °C). Besides the choice of electrolyte material, there are many issues needed to be addressed in order to make oxygen sensors of high performance (namely, high sensitivity and selectivity, fast response, high reliability and stability) [1-12]. For instance, the electrochemical properties of the electrolyte are quite sensitive to processing and microstructure. Moreover, the electrochemical processes occurring at the electrode interfaces also play an important role in the performance of gas sensors. Slow electrode kinetics are often found to be responsible for unsatisfied device performance such as slow response, especially at lower temperatures [3-18]. The electrodes for gas sensors should have high electrical conductivities, high catalytic activities, adequate porosity for gas transport, good compatibility with the electrolyte, and long-term stability [3-11]. In order to achieve high catalytic activities, it is preferred that the electrodes be highly porous so that it retains a large number of active sites for electrochemical reactions, i.e., the triple-phase points or triple-phase boundaries. All the above factors offer great opportunities of performance optimization through modification of processing and microstructure. During Phase I, NRC aimed to established the proof-of-concept for developing low-temperature, low power consuming, miniaturized oxygen sensors based on YSB materials.

The objectives of the Phase I work included fabricating an oxygen sensor based on YSB nanomaterials, characterizing the sensor components (the electrolyte and the electrodes), testing the sensor, and developing the conceptual basis for a systematic development and optimization work during Phase II. During Phase I, we have studied basic dependence of properties on material, processing, and

microstructure of the sensor components, and have identified electrode kinetics as a major performance-limiting factor. Then we have focused on significantly improving the sensor performance by introducing nanostructured composite electrodes. The nanostructured sensors have been evaluated extensively. Phase I results suggest that NRC's nanostructured sensors outperform the base line sensors, and that nanostructured materials are excellent foundation for electrode and electrolyte processing for physiological applications. Nanocomposite electrodes were found to be 400% better than conventional technology, and the proof-of-concept sensing device made from nano-YSB and nanocomposite electrodes was found to be fully functional even at temperatures that are 100°C less than the best achievable by competing technologies. The lower temperature can significantly reduce power requirements and extend battery life. The Phase I effort, in summary, successfully demonstrated the proof-of-concept. The following sections outline results of the Phase I work.

## 2. WORK DONE FOR THE PHASE I PROGRAM

### 2.1. Synthesis of nanosized YSB powder

Different chemicals, including bismuth chloride ( $\text{BiCl}_3 \cdot \text{H}_2\text{O}$ ), bismuth nitrate ( $\text{Bi}(\text{NO}_3)_3 \cdot 5\text{H}_2\text{O}$ ), yttrium oxide ( $\text{Y}_2\text{O}_3$ ), and yttrium nitrate ( $\text{Y}(\text{NO}_3)_3 \cdot 6\text{H}_2\text{O}$ ), were studied as precursors for preparing nanosized YSB powder via solution co-precipitation.

Initially, bismuth chloride ( $\text{BiCl}_3 \cdot \text{H}_2\text{O}$ ) and yttrium oxide ( $\text{Y}_2\text{O}_3$ ) were used as precursors to prepare first batches of nanosized YSB powder. The molecular ratio of bismuth chloride to yttrium oxide was 6 : 1 to make the powder have a composition of  $\text{Bi}_{1.5}\text{Y}_{0.5}\text{O}_3$ . When  $\text{BiCl}_3 \cdot \text{H}_2\text{O}$  was placed into water, it instantaneously formed a hydroxide colloidal suspension. Therefore nitric acid was required to facilitate the dissolution of the suspension. The solubility of  $\text{Y}_2\text{O}_3$  in water was also low. In a quite acid solution with a pH of about 1, prolonged time (more than 12 hours) was required to obtain a clear solution. Then the Bi-Y solution was diluted with ethanol, and slowly added to a basic solution of ammonium hydroxide, and precipitation successfully took place instantaneously. The precipitate was then filtered, washed, dried, and calcined at 500°C in air to form fine-grained YSB powder. The calcined powder was redispersed in water by ultrasonication to break up weak agglomerates formed during the heat treatment. However, we observed that it was very difficult to prepare single-phased YSB nanopowder in this way. In the attempt of obtaining the right phase, we calcined the powder under different conditions (at 500°C for 2 hours; at 650°C for 20 minutes; and at 800°C for 20 minutes). But X-ray diffraction (XRD) analysis consistently showed that the powder fired under these conditions does not have a single cubic phase. Instead, it showed mixed phases with unknown XRD peaks, as shown in Figure 1.

High quality YSB nanopowder was prepared with bismuth nitrate and yttrium nitrate precursors. Figure 2 shows the flow chart of the co-precipitation processing. After precipitation, the precipitate solution was suction filtered, and the gelatinous filter cake was washed in acetone to minimize agglomeration of ultrafine powder due to hydrogen bonding. The loose powder so generated was next dried with mild heating to remove water and acetone. Then the powder was calcined in air at 400°C for

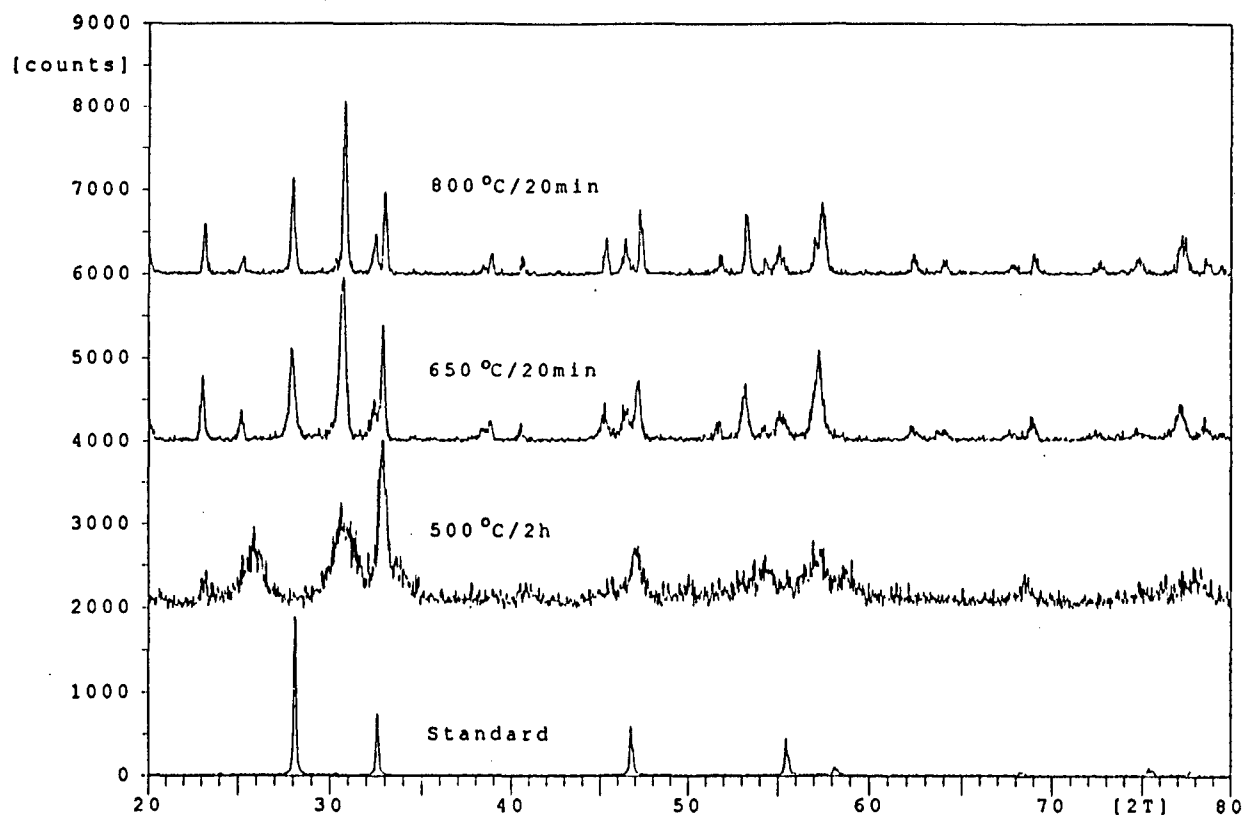


**Figure 1.** XRD patterns of YSB nanopowders prepared from bismuth chloride and yttrium oxide.

2 hours and at 500°C for 2 hours, respectively. XRD showed that both calcine schedules resulted in a single cubic YSB phase (Figure 3). It is clear that using nitrates for preparation the YSB nanopowder is the right synthesis protocol. 500°C seems to be a suitable calcine temperature, while 400°C may be too low to yield good crystallinity (as indicated by the ragged XRD pattern). The volume averaged crystallized size of the powder fired at 500°C was determined to be 12.5 nm by analyzing the broadening of the (111) diffraction peak and applying Scherrer's formula.

The YSB nanopowder prepared with nitrate precursors was characterized in terms of morphology and particle size by transmission electron microscopy (TEM). Shown in Figure 4 is a TEM image of the nanopowder prepared by co-precipitating bismuth nitrate and yttrium nitrate (calcined at 500°C for 2 hours). From the image, the average particle size was estimated to be about 15 nm, which is in good agreement with the result obtained from XRD analysis.



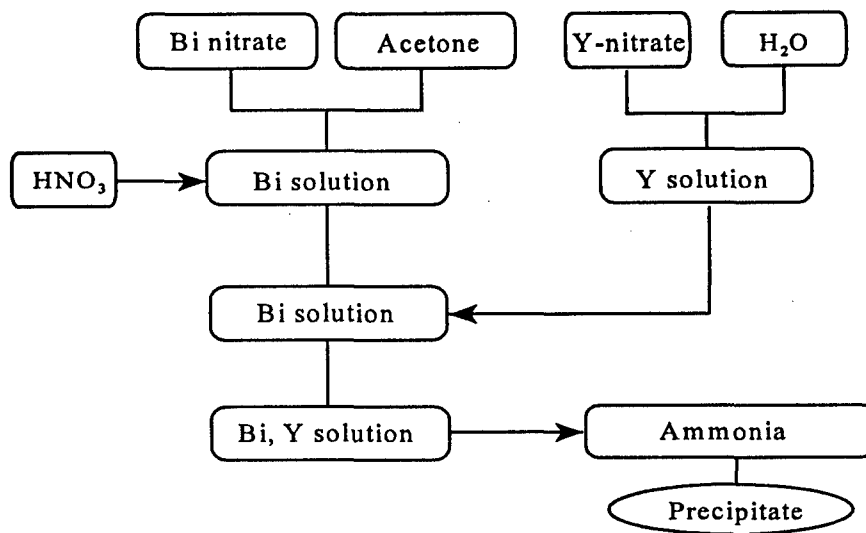


Figure 2. Flow chart for preparation of YSB nanopowder by a solution method from nitrates.

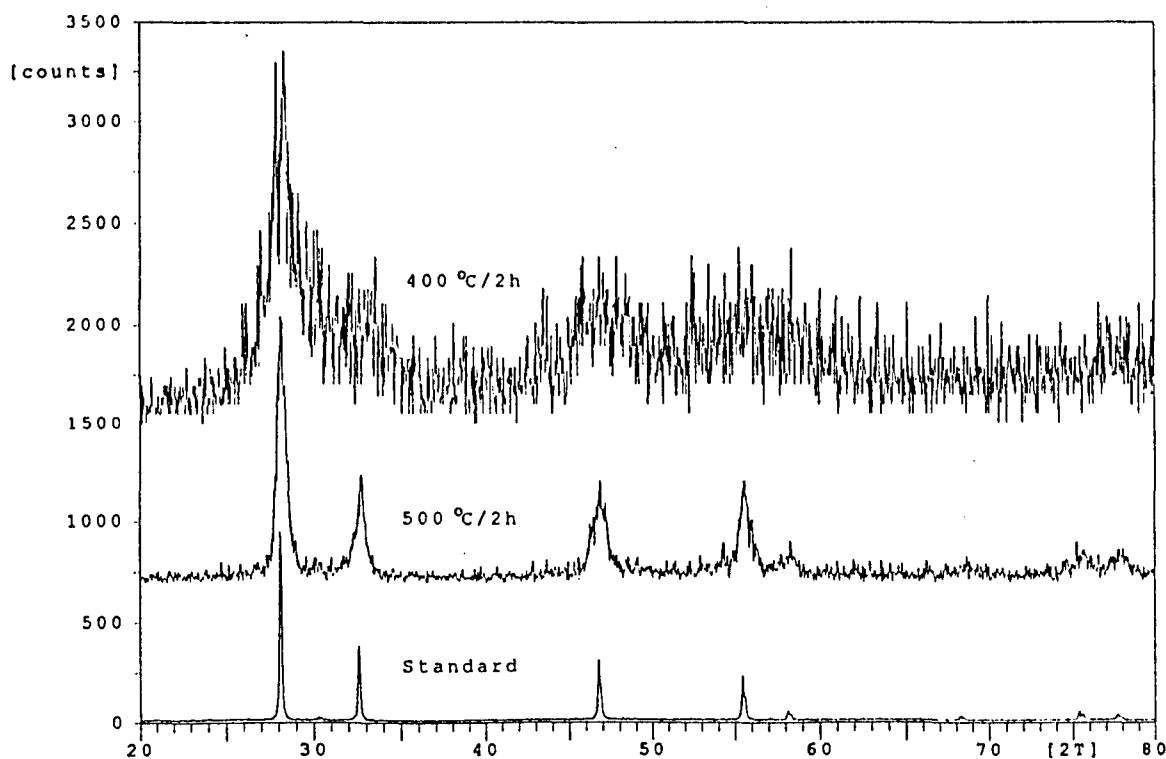
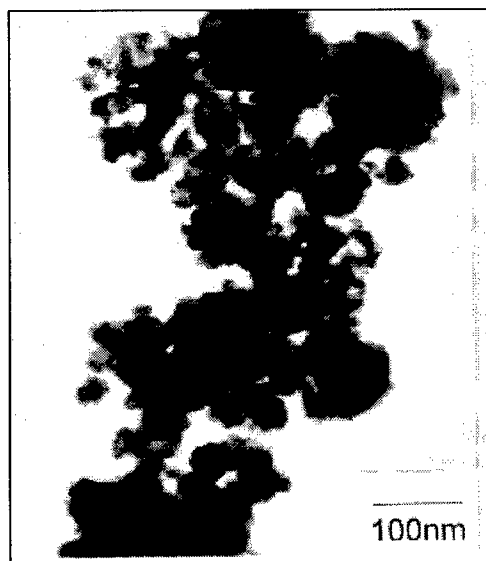


Figure 3. XRD patterns of YSB nanopowders prepared from bismuth nitrate and yttrium nitrate.



**Figure 4.** TEM image of YSB nanopowder prepared from bismuth nitrate and yttrium nitrate.

## 2.2. Processing of YSB electrolytes

The nanopowders were uniaxially pressed at about 50000 psi into green pellets of two sizes: 12.5 mm in diameter and 1 mm in thickness (used for electrochemical characterization), and 25 mm in diameter and 1.2 mm in thickness (used for assembling the testing sensor for performance evaluation). The pressing process consisted of initially lubricating the die with a die lube (from Marjon Ceramics, Tucson, AZ), followed by the weighing out appropriate amount of powder, inserting the powder in the die, pressing to the desired pressure, holding at the pressure for 30 seconds, and then slowly releasing the pressure over 15 seconds. Subsequently, the pellet was forced out from the die. No binder was added for the forming process.

Different sintering conditions have been investigated in order to prepare YSB electrolytes of high quality. It was found that from the nanopowder the electrolytes can be sintered with greater than 96 % of theoretical density at temperatures ranging from 850 to 950°C. In contrast, YSB electrolytes made from micron-sized powder are typically sintered at temperatures greater than 1000°C. It is known that the primary driving force for densification of ceramics is the reduction of free surface area at high temperatures. The very small size of the YSB nanopowder therefore has a very large driving force for densification, and thus the required sintering temperature can be significantly reduced relative to commonly used micron-sized powders. Shown in Figure 5 are XRD patterns of YSB electrolyte pellets sintered from nanopowder at 850°C for 4 hours and 950°C for 4 hours, respectively. Although both patterns show a single cubic YSB phase, the pellets sintered at the higher temperature appeared to be more mechanically robust. Therefore, the electrolytes have been prepared by sintering at 950°C for 4

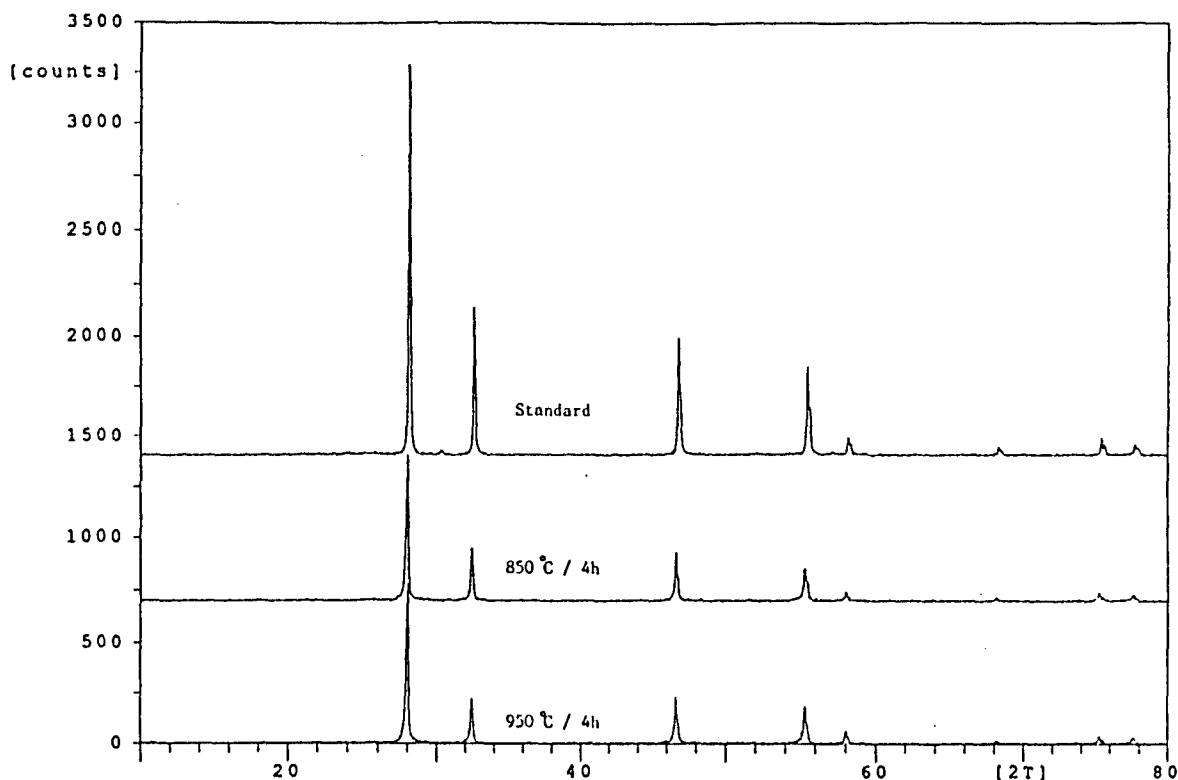


Figure 5. XRD patterns of YSB electrolytes prepared from YSB nanopowder.

hours for all electrochemical measurements and sensor performance evaluation in the Phase I work.

### 2.3. Electrochemical characterization of conventional Ag|YSB|Ag cells

In order to determine the critical factors which limit the sensor performance and further to identify the most effective approaches to significantly enhancing the sensor performance, we have conducted a series measurements with conventionally-processed Ag|YSB|Ag cells. Shown in Figure 6 is a Nyquist plot of impedance spectrum of a measured at 475°C in air. Generally, the intercept of the impedance loop with the real axis at high frequencies corresponds to the resistance of the electrolyte,  $R_b$ , and the intercept of the impedance loop with the real axis at low frequencies corresponds to the total resistance of the cell,  $R_T$ . The interfacial polarization resistance of the electrodes,  $R_e$ , therefore, is represented by the difference of the two intercepts, i.e., [1,2]

$$R_e = R_T - R_b$$

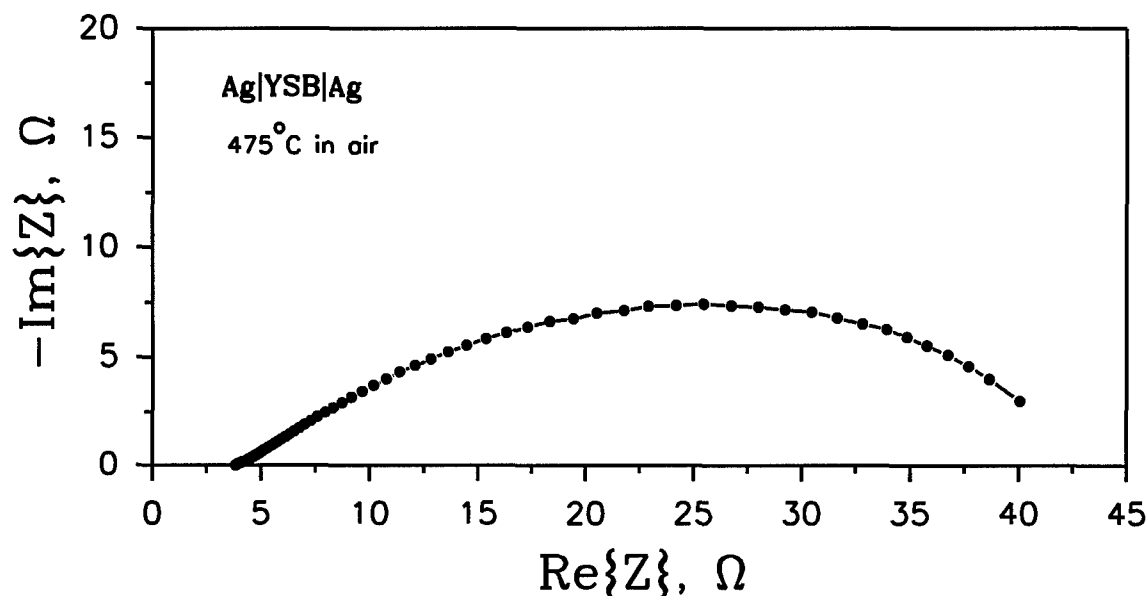


**Figure 6.** Impedance spectrum of a conventionally-processed Ag|YSB|Ag cell measured at 475°C in air. The electrolyte thickness is 0.07cm and the electrode area is 0.78 cm<sup>2</sup>.

Figure 6 clearly shows that the polarization resistance of the electrodes ( $R_e$ ) is much larger than the electrolyte resistance ( $R_b$ ). The data suggests that, at the temperature range being studied (400-650°C), which is much lower than the operating temperatures of YSZ oxygen sensors, the electrode kinetics is an important issue that needs to be addressed for achieving high performance of the sensor.

This assertion was further supported by the results of a systematic electrochemical characterization of the conventional Ag|YSB|Ag cells. Shown in Figure 7 are electrode and electrolyte resistances of the cell as a function of temperature, measured in air. It is clear that, in the temperature range tested, the electrode resistance is much larger than the electrolyte resistance. This indicates that the electrode kinetics is the limiting factor to the sensor performance. Therefore enhancing electrode kinetics would be the most effective way to enhance the sensor performance. Figure 8 further shows the dependence of the electrode overpotential and the IR drop of the electrolyte of the cell on current density passing through the cell. At low current densities, the electrode overpotential dominates over the IR drop of the electrolyte. This again indicates that the sensor performance is mainly limited by electrode kinetics, since the oxygen sensor is operated in potentiometric mode, in which the current passing through the cell is close to zero. The electrode effect will be even more significant as the thickness of

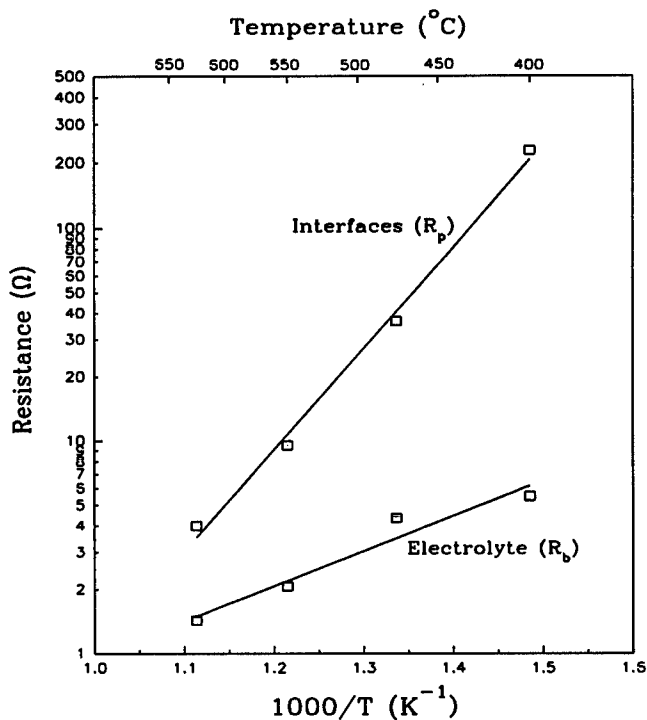


Figure 7. electrode and electrolyte resistances of a Ag|YSB|Ag cell as a function of temperature, measured in air. The electrode area is 0.78 cm<sup>2</sup> and the electrode thickness is 0.07 cm.

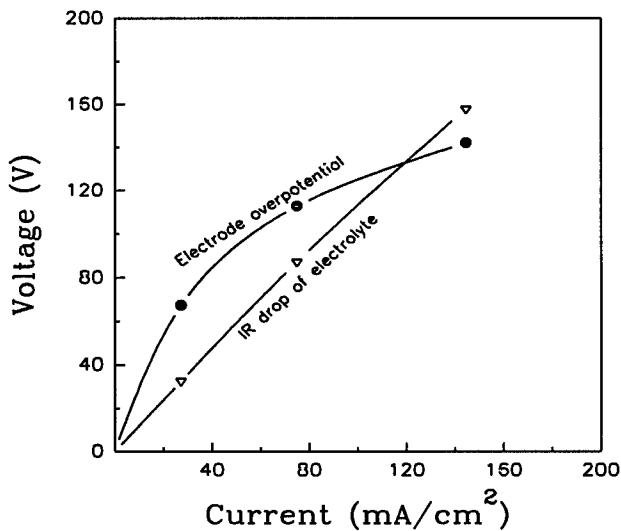
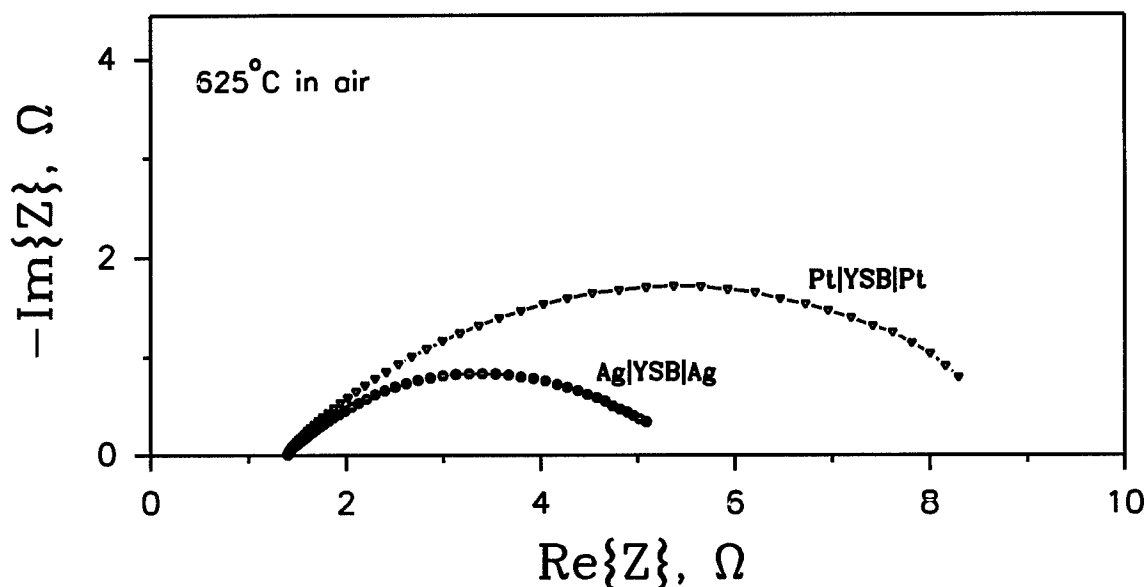


Figure 8. I-V characteristics of the Ag|YSB|Ag cell, measured at 625°C in air.



**Figure 9.** Impedance spectra of a Ag|YSB|Ag cell and a Pt|YSB|Pt cell measured at 625°C in air. The electrolyte thickness is 0.07cm and the electrode area is 0.78 cm<sup>2</sup>.

the electrolyte is reduced and as the operating temperature is lowered [1-6].

A comparison has been made for silver electrode and platinum electrode. Shown in Figure 9 are impedance spectra of a Ag|YSB|Ag cell and a Pt|YSB|Pt cell (both were conventionally-processed) measured at 625°C in air. Clearly, the Ag electrodes show a lower polarization resistance than the Pt electrodes. This indicates that, in the present case, using Ag-based electrodes is a better choice than using Pt-based electrodes as far as minimizing the polarization resistance is concerned, not to mention Ag is much cheaper than Pt. Nevertheless, the polarization resistances of the Ag electrodes are still too large, and special attention was paid in the Phase I work to enhance the electrode kinetics. Given the importance of this to the proof-of-concept, modification of Ag-based electrodes was initiated and explored in the Phase I work.

#### 2.4. Modification of Ag-based electrodes

Electrodes for oxygen sensors should have high electrical conductivities, high catalytic activities, adequate porosity for gas transport, good compatibility with the electrolyte, and long-term stability. In

order to achieve high catalytic activities, it is preferred that the electrodes be highly porous so that it retains a large number of active sites for electrochemical reactions, i.e., the triple-phase points or triple-phase boundaries [1,3,4]. Ag has been studied as an electrode material since it is known to have high electrical conductivity and high catalytic activity for oxygen reduction and evolution. However, pure Ag electrodes readily densify during processing and operation, resulting in a dense electrode with little porosity [1]. Figure 10 shows a SEM photograph of a typical view of the pure Ag electrodes. The nearly pore-free, dense microstructure seems to account for the high electrode resistances of the Ag|YSB|Ag cells.

In order to reduce the electrode resistances, we have studied Ag-YSB composite electrodes. In the composites, the densification of the Ag phase is inhibited by the ceramic phase. The electrodes then retain a porous microstructure while the sensors undergo thermal tensions during processing and operation, as shown in Figure 11. The retained porous microstructure is expected to significantly enhance the performance of the electrodes. In addition, electrodes of this kind should have better adhesion to the



**Figure 10.** SEM surface view of a pure Ag electrode on the YSB electrolyte.

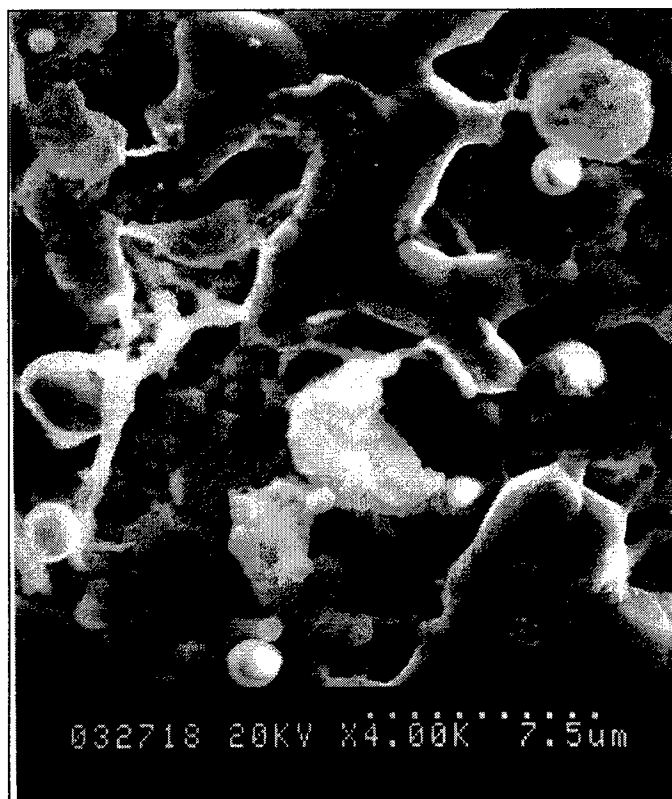


**Figure 11.** SEM surface view of a Ag-YSB composite electrode (containing 85 v % of Ag) on the YSB electrolyte.

electrolytes, since the stress arising from thermal expansion mismatch between the ceramic electrolyte and the metal electrode is minimized not only by the porous, heterogeneous microstructure of the electrodes but also by tailoring the thermal expansion coefficient of the composites. Further, there is still another potential advantage with using the composite electrodes. If the ceramic phases added are ionic conductors or mixed electronic-ionic conductors, the composite electrodes as a whole may turn out to be a mixed conductor, which allows ambipolar transport within the solid phase and hence is generally favored for catalytic electrodes.

Shown in Figure 12 are Nyquist plots of impedance spectra of cells with the composite electrodes in comparison with a cell with pure Ag electrodes. As determined from the impedance spectra, the polarization resistances of the composite electrodes are significantly smaller than that of the pure Ag electrode. As expected, the resistance of the composite electrode is a function of the composition, i.e., the volume fraction of each constituent phase. This allows much room for performance optimization by adjusting the composition of the composites. The nanocomposite electrode containing 15 % ceramic



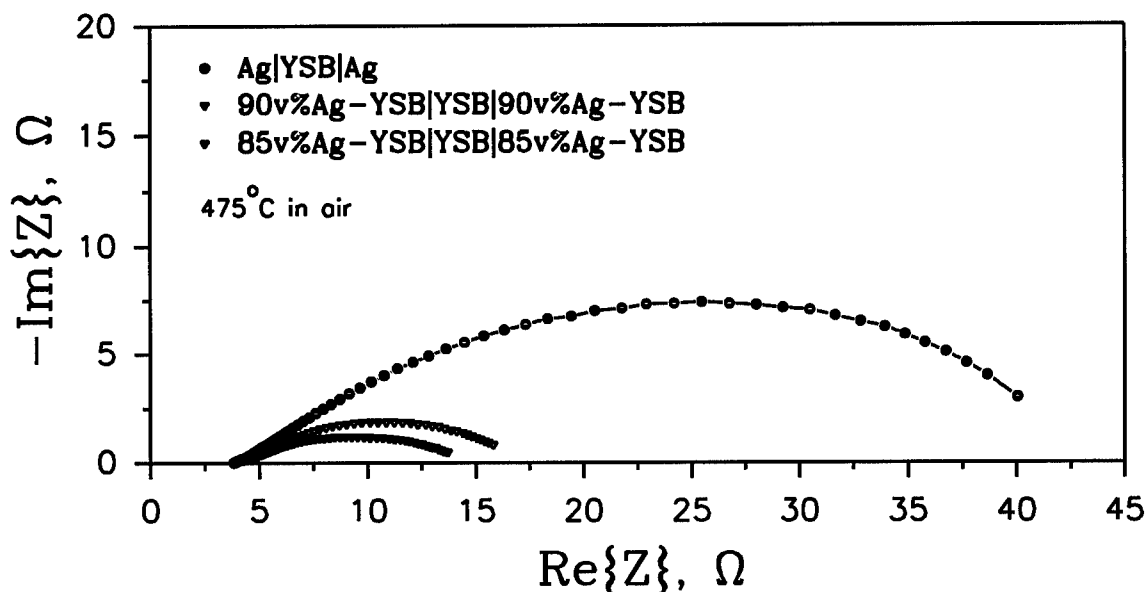


**Figure 12.** Impedance spectra of different cells measured at 475°C in air. The electrolyte thickness is 0.07cm and the electrode area is 0.78 cm<sup>2</sup>.

phase shows a nearly 4-fold reduction in electrode resistance as compared to the pure Ag electrode. This is a very encouraging result, especially because this was achieved without any composition optimization. We believe that with composition optimization, further reduction in electrode resistance can be achieved, leading to a significant enhancement in sensor performance.

Figure 13 further shows electrode resistances of the nanocomposite electrodes as a function of temperature, as determined from the impedance spectra measured in air. Also shown in the figure are the data for pure Ag electrode for comparison. As compared with pure Ag electrode, the nanocomposite electrodes show significantly lower resistances. Figure 14 compares electrode overpotentials as a function of current passing through the cell between a cell with composite electrodes and a cell with pure Ag electrodes. Again, at the same currents, the nanocomposite electrodes show much lower overpotentials than the pure Ag electrodes. Based on these results, it can be concluded that using Ag-YSB composite electrodes is much preferred than using pure Ag electrodes for the YSB oxygen sensor. Also, as shown in Figure 13, the electrode resistance of the composite electrode is a strong function of the composition. This suggests that the sensor performance can be optimized through the composition optimization of the composite electrodes in Phase II.

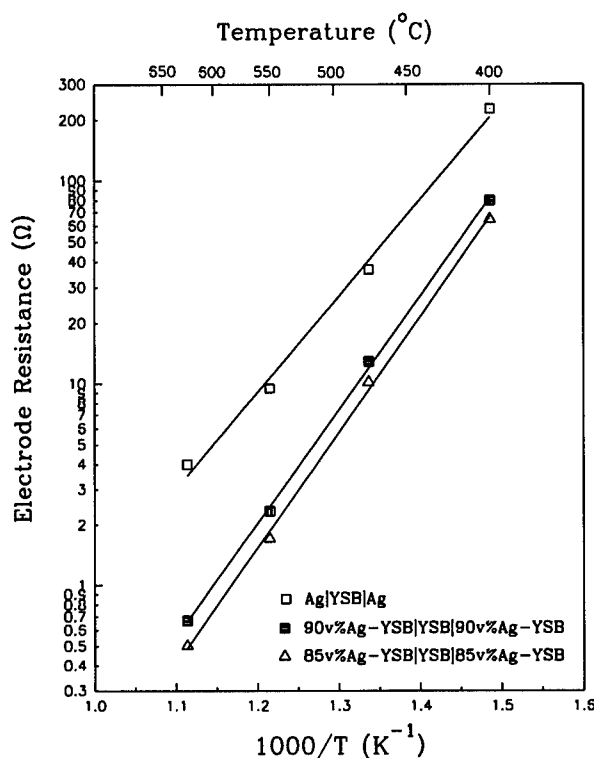


**Figure 13.** Resistances of different electrodes as a function of temperature, as determined from impedance spectra measured in air. The electrode area is  $0.78 \text{ cm}^2$ .

## 2.5. Characterization of YSB electrolytes made from YSB nanopowder

Shown in Figure 15 are a series of impedance spectra of the cell using the YSB electrolyte made from nanopowder with pure Ag electrodes, measured at different temperatures in air. The impedance spectra of this type of cells are not much different from those measured from the cell using the YSB electrolyte made from micron-sized powder with the same type electrode, as shown in Figure 16. This indicates that the grain size of the YSB powder has little effect on the ionic conductivity of the sintered YSB electrolyte and the electrochemical characteristics of the electrolyte-electrode interfaces. This further suggests that electrode modification (surface micro-engineering) is a greater opportunity for prepare high performance oxygen sensors. On the other hand, the ionic conductivity of the YSB electrolyte is about two orders of magnitude higher than that of YSZ electrolyte, as shown in Figure 17. This is what has been expected.

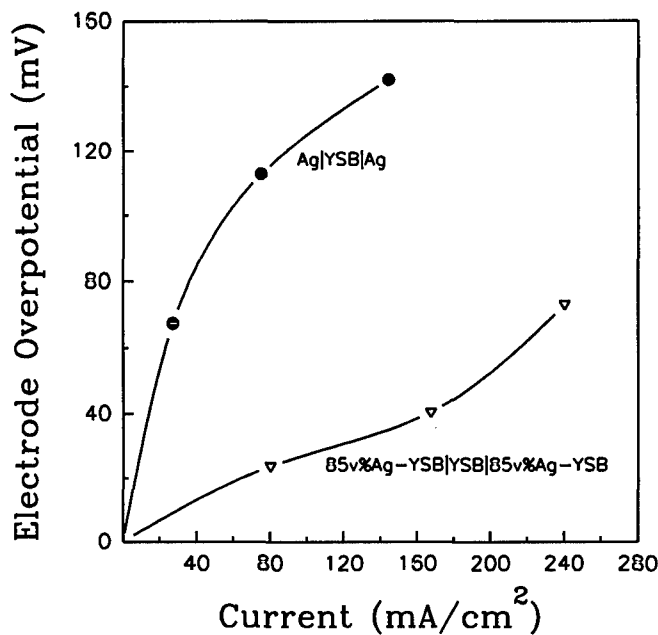


Figure 14. The overpotentials of different electrodes as a function of the current passing through the cell.

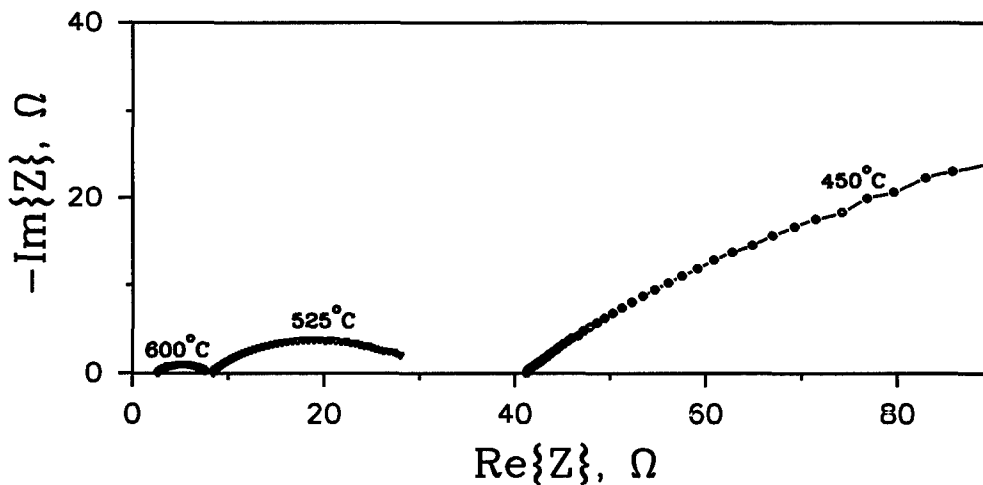


Figure 15. Impedance spectra of a cell using YSB electrolyte made from nanopowder and Ag electrodes, measure at different temperatures in air. The electrolyte thickness is 0.07 cm and the electrode area is 0.5 cm².

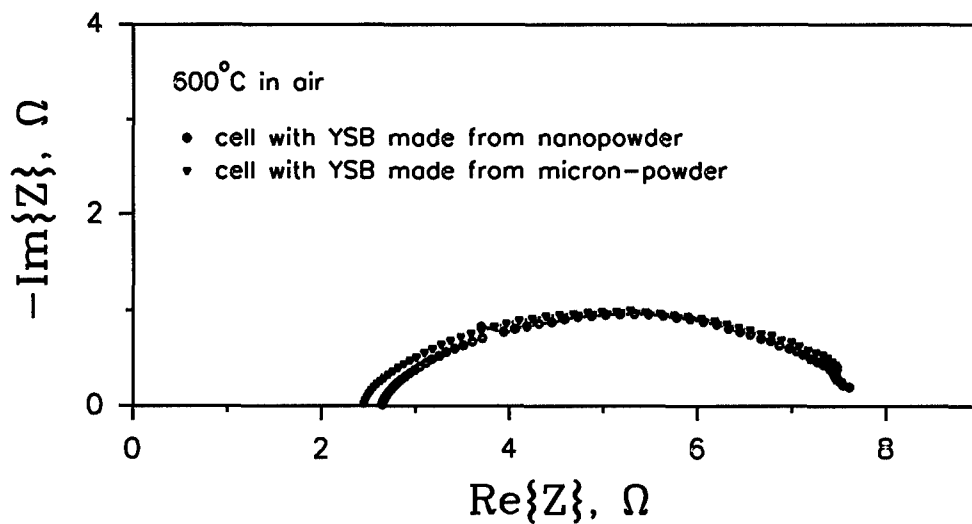


Figure 16. Comparison of impedance spectra from cells of two types of YSB electrolytes.

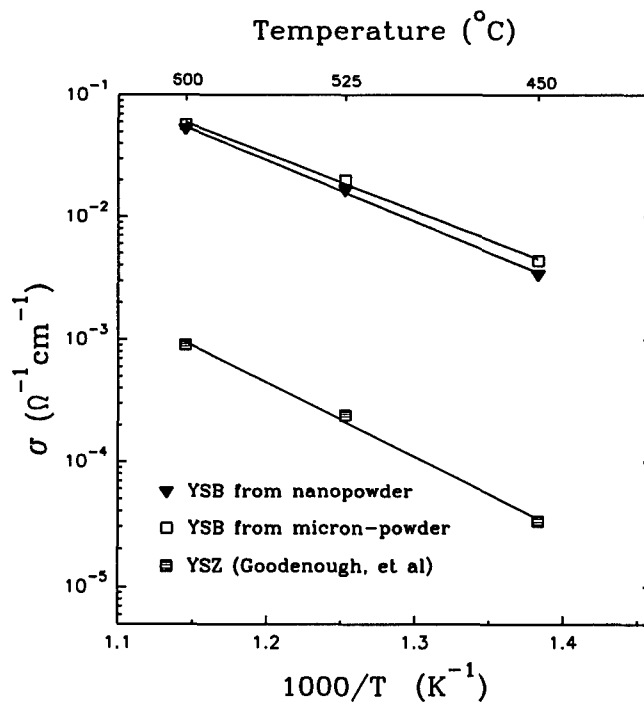


Figure 17. Ionic conductivity of YSB electrolytes in comparison with YSZ electrolyte.

## **2.6. Construction of the sensor testing system**

The comprehensive testing system for various solid-state electrochemical components and devices, including sensors, was assembled in NRC in the Phase I work. A schematic diagram of the system design is shown in Figure 18 and is described as follows.

The test sensor consisted of an electrolyte and electrodes on both sides. Silver wire were attached to the electrodes for making the electrical measurements. The test sensor was sealed between two alumina tubes with a sealing glass, thereby creating two separate chambers so that the sensor is exposed to different gases on the two sides. One chamber was filled with the sensing gas while the other will be filled with a reference gas, which is typically air. If air was used as the reference, the second chamber was not necessary since one side of the sensor can simply be exposed to ambient air. Yet the two-chamber configuration allowed sensor test in a variety of gas combinations, and extensive electrochemical characterization of sensors and other solid state electrochemical devices such as fuel cells and oxygen pumps. Obviously, hermetic glass seals between the sample and the alumina tubes were crucial to reliable sensor testing.

The sensor assembly was placed in a tube furnace, which was controlled by a programmable temperature profile controller to ensure desired heating, soaking, and cooling control. A computerized electrochemical measurement system, consisting of Solartron 1260 (impedance/phase-gain analyzer) and 1287 (electrochemical interface), was used for measuring the electrochemical properties of different sensor components (the electrolyte and the electrodes) and the performance of the sensor.

The gas supply was furnished with a sophisticated gas control system equipped with four MKS electronic mass flow controllers. This system was capable of providing gas mixtures of different oxygen partial pressures with precisely controlled flow rates. The two gas feeds can be easily switched between the two lines without the need of disconnecting and reconnecting any fitting along the lines, so that a most reliable control of the gases was ensured.

The partial pressures of oxygen in the inlet gases and outlet gases are further monitored by four oxygen sensors. The monitoring of the outlet gases was an additional feature to the sensor test, while it was necessary for the test of oxygen pump and oxygen permeation devices.

As mentioned above, identifying suitable glasses for making hermetic seals was the key to preparing a reliable, high performance sensor cell. The requirements for the glasses in this case include strong binding with both alumina support tube and the YSB electrolyte material, no chemical reaction between the glass and the YSB electrolyte, and suitable thermal expansion coefficient (in between that of alumina and that of YSB). In Phase I work, we have conducted an extensive search for the sealing glasses. Six glasses have been tested, and two of them (VHX-57 and VTS-9 from Vitrifunctions) have been identified as suitable glasses for assembling the sensors in this project.

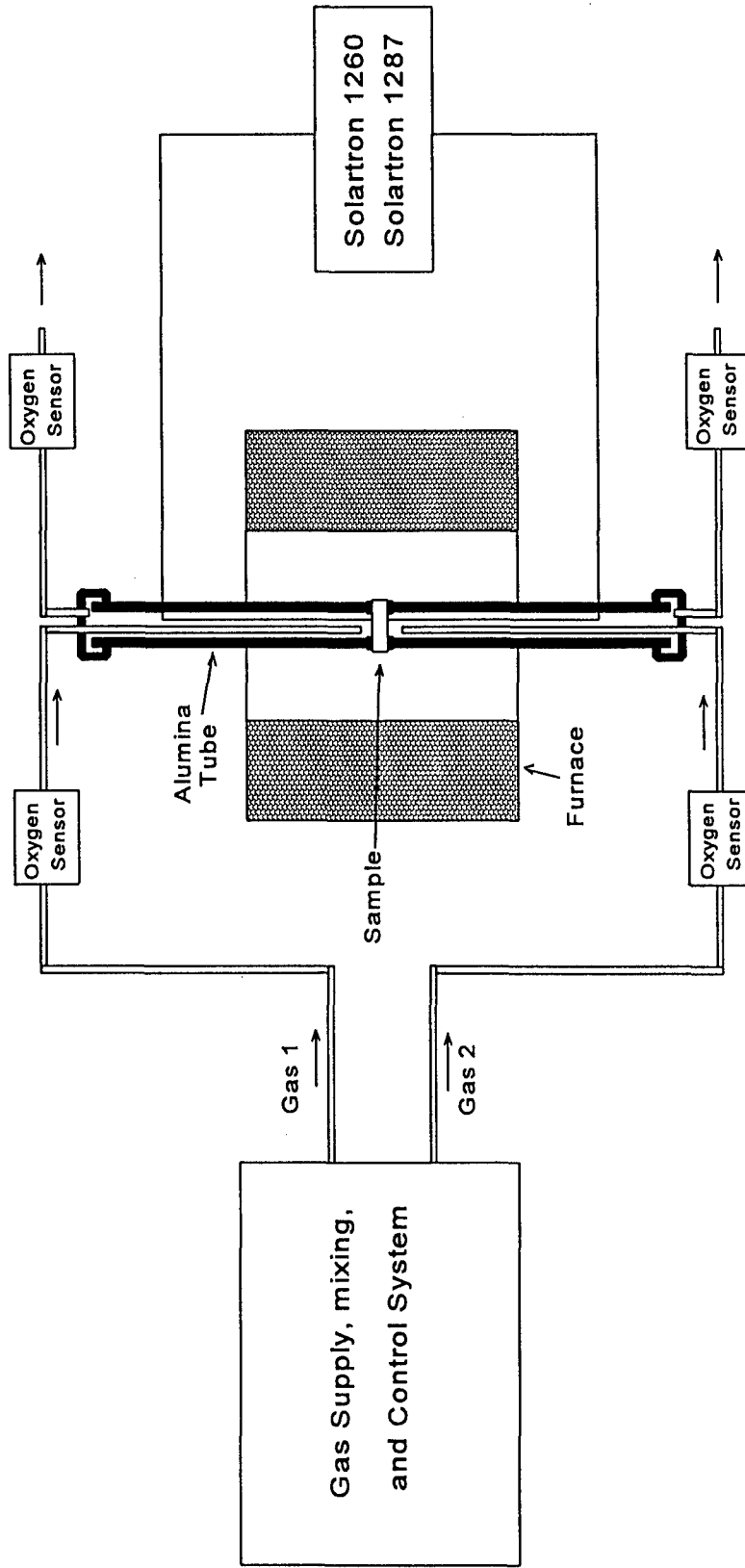


Figure 18. Schematic diagram of the sensor testing system.

## 2.7. Evaluation of sensor performance

YSB electrolyte pellets of about 19 mm in diameter and about 0.9 mm in thickness (sintered from green pellets of 25 mm in diameter and 1.2 mm in thickness) were used for sensor test. The pellets were ground and polished to a thickness of 0.7 mm. A composite paste of 79v%Ag21v%YSB, prepared by mixing nanopowder of YSB and unfritted Ag paste (Heraeus: C4400UF), was printed onto both sides of the pellet, and consequently the pellet was fired at 800°C for 10 minutes to form a sensor cell with porous composite electrodes. Then Ag wire was attached to both electrodes with a contact of Ag epoxy which was fired at 730°C for 2 minutes. The testing sensor was constructed by sealing this cell to an alumina support tube (shown in Figure 18) with the glasses (VHS-57, or VTS-9). Air was used as the reference gas, and therefore the second alumina tube was not used. The sensor was operated in the configuration of

air, 79v%Ag21v%YSB | YSB | 79v%Ag21v%YSB, Analyte gas

The sensor response to the changes in the gas composition and in temperature was monitored by measuring the cell voltage in different conditions.

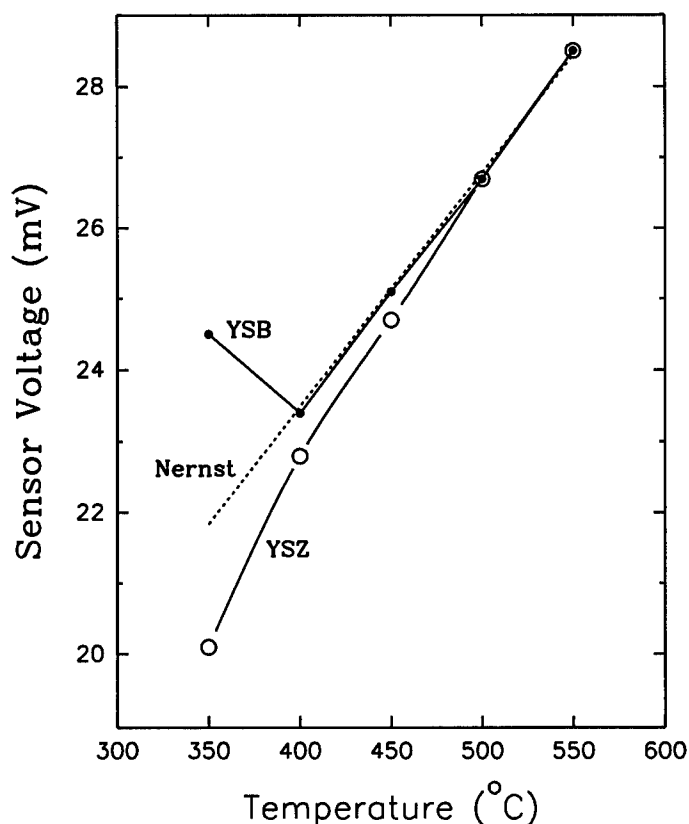


**Figure 19.** Voltage response of a YSB sensor in oxygen as a function of temperature in comparison with that of a YSZ sensor. The reference gas is air.

Shown in Figure 19 is the sensor voltage response in oxygen as a function of temperature in comparison with that of a conventional YSZ sensor. Also shown in the figure is, as a reference line, the Nernst response calculated by:

$$E = \frac{RT}{4F} \ln\left(\frac{P_{O_2, \text{oxygen}}}{P_{O_2, \text{air}}}\right)$$

where E is the Nernst voltage, R the gas constant, T the temperature in Kelvin, F is Faraday's constant,  $P_{O_2, \text{oxygen}}$  and  $P_{O_2, \text{air}}$  are the oxygen partial pressures in the analyte gas and in the reference gas respectively. Figure 19 clearly shows that the response of the YSB sensor follows Nernst behavior down to 400°C, while the response of the YSZ sensor deviates from Nernst behavior below 500°C. This indicates that the YSB proof-of-concept sensor can be operated at a temperature about 100°C lower than the conventional YSZ sensor.

Shown in Figure 20 is the sensor response to changes in gas composition at 450°C. At this low temperature, the response speed of the sensor depends on the oxygen partial pressure of the analyte gas. In gases of relatively high oxygen partial pressure, the sensor responds quite rapidly, as in the case of air

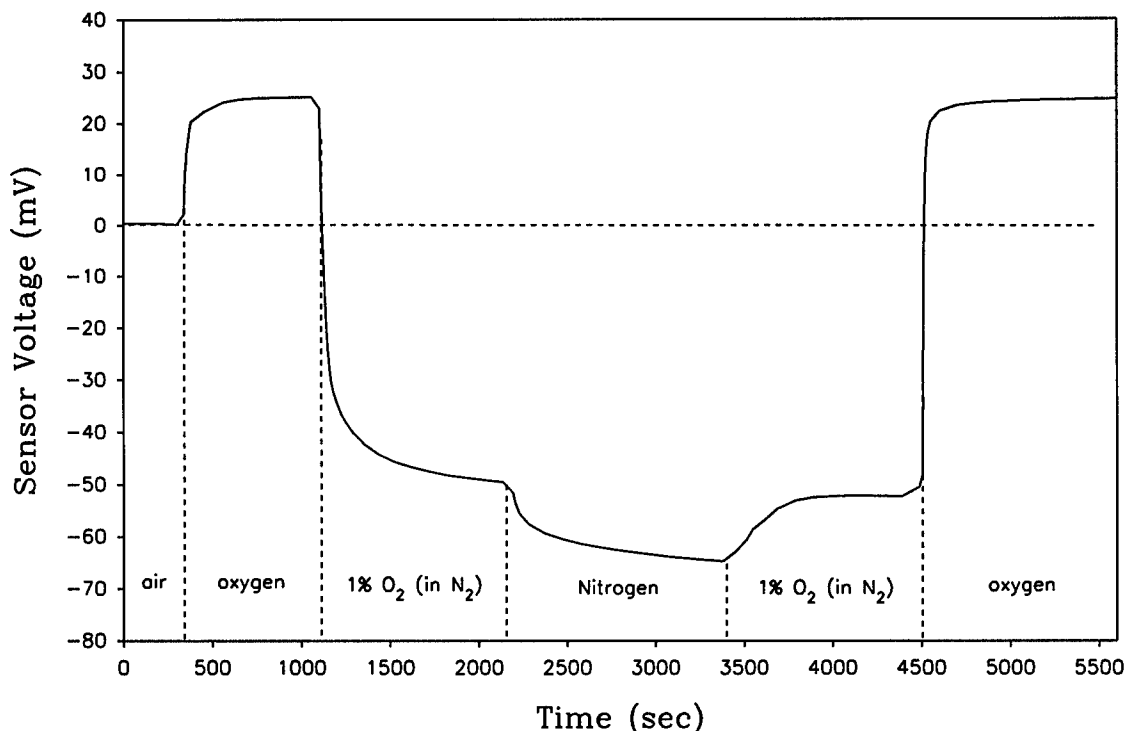


**Figure 20.** Response of the YSB sensor to changes in gas composition at 450°C, with reference to air.



and oxygen. In gases of relatively low oxygen partial pressure, the sensor response seems to be slow and sluggish. These results clearly indicate that enhancing the electrode kinetics, especially in gases of low oxygen partial pressure, is the key to improving the sensor performance at low temperatures. This should be the central task in the optimization work during Phase II.

### 3. CONCLUSIONS

- Nanoscale YSB powder with an average particle size of about 15 nm can be successfully synthesized via solution precipitation, using nitrates as precursors.
- Nanopowder of YSB can be processed into sensor electrolytes without binders and at significantly lower sintering temperatures.
- A systematical characterization of conventionally-processed Ag|YSB|Ag cells indicates that Ag-based electrodes are more catalytically active than Pt-based electrodes, and that electrode kinetics is the limiting factor to the sensor performance.
- Modification and nano-engineering of the electrodes offers a great opportunity of performance enhancement of the oxygen sensors. Using Ag-YSB nanocomposite electrodes instead of pure Ag electrodes can significantly enhance electrode kinetics of YSB sensors and hence the sensor performance.
- Ionic conductivity of the YSB electrolyte is much higher than that of YSZ electrolyte. Grain size of the YSB powder has little effect on the ionic conductivity of the sintered YSB electrolyte and the electrochemical characteristics of the electrolyte-electrode interfaces.
- YSB sensors with Ag-YSB composite electrodes can be operated at a temperature about 100°C lower than the conventional YSZ sensor. Further enhancing electrode kinetics of the sensors, especially in gases of low oxygen partial pressure, is the key to improving the sensor performance at low temperatures.
- The sensor testing system set up at NRC is a powerful technique for evaluating sensor performance under operating conditions.
- VHX-57 and VTS-9 from Vitrifunctions are suitable glasses for assembling the sensors in this project.

In summary, the tasks planned for the Phase I of this project have been completed, and the proof-of-concept of developing low-temperature, low power consuming, miniaturized oxygen sensors based on YSB materials has been successfully demonstrated.

### 4. REFERENCES

1. H. Hu and M. Liu, *J. Electrochem. Soc.*, 143, 859 (1996).
2. M. Liu, H. Hu, and W. Rauch, in *Proceedings of 1st International Symposium on Ceramic Membranes*, H. Anderson et al, Editors, The Electrochemical Society, Pennington, NJ (in press).
3. H. L. Tuller and P. K. Moon, *Mater. Sci. and Eng.*, B1, 171 (1988).

4. S. Liou and W. L. Worrell, in *Proceedings of 1st International Symposium on SOFC*, S. C. Singhal, Editor, PV 89-11, p.81, The Electrochemical Society Proceedings Series, Pennington, NJ (1989).
5. N. Bonanos, B. Ellis, K. S. Knight, and M. N. Mahmood, *Solid State Ionics*, 35, 179 (1989).
6. B. A. Van Hassel, B. A. Boukamp, and A. J. Burggraaf, *Solid State Ionics*, 53-56, 890 (1992).
7. D. R. Franceschetti and J. R. Macdonald, *J. Electroanal. Chem. Interfacial Electrochem.*, 82, 271 (1977).
8. R. C. T. Slade and N. Singh, *Solid State Ionics*, 46, 111 (1991).
9. A. V. Virkar, *J. Electrochem. Soc.*, 138, 1481 (1991).
10. M. Liu, in *Proceedings of 1st International Symposium on Ionics and Mixed Conducting Ceramics*, T. A. Ramanarayanan and H. L. Tuller, Editors, PV 91-12, p. 191, The Electrochemical Society Proceedings Series, Pennington, NJ (1991).
11. T. W. Kueper, S. J. Visco, and L. C. De Jonghe, *Solid State Ionics*, 52, 251 (1992).
12. M. Liu and A. Khandkar, *Solid State Ionics*, 52, 3 (1992).
13. A. F. Sammells, R. L. Cook, J. H. White, J. J. Osborne, and R. C. MacDuff, *Solid State Ionics*, 52, 111 (1992).
14. L. S. Wang and S. A. Barnett, *J. Electrochem. Soc.*, 139, 1134 (1992).
15. C. C. Chen, M. M. Nasrallah, and H. U. Anderson, *J. Electrochem. Soc.*, 140, 3555 (1993).
16. M. Feng, J. B. Goodenough, *Solid State Ionics*, 68, 269 (1994).
17. G. B. Barbi and C. M. Mari, *Solid State Ionics*, 6, 341 (1982).
18. H. Hu and M. Liu, in *The Role of Ceramics in Electrochemical Devices*, P. N. Kumta, G. S. Rohrer, and U. Balachandran, Editors, in press, (1995).



DEPARTMENT OF THE ARMY  
US ARMY MEDICAL RESEARCH AND MATERIEL COMMAND  
504 SCOTT STREET  
FORT DETRICK, MARYLAND 21702-5012

REPLY TO  
ATTENTION OF:

MCMR-RMI-S (70-1y)

4 Dec 02

MEMORANDUM FOR Administrator, Defense Technical Information  
Center (DTIC-OCA), 8725 John J. Kingman Road, Fort Belvoir,  
VA 22060-6218


SUBJECT: Request Change in Distribution Statement

1. The U.S. Army Medical Research and Materiel Command has reexamined the need for the limitation assigned to technical reports written for this Command. Request the limited distribution statement for the enclosed accession numbers be changed to "Approved for public release; distribution unlimited." These reports should be released to the National Technical Information Service.

2. Point of contact for this request is Ms. Kristin Morrow at DSN 343-7327 or by e-mail at Kristin.Morrow@det.amedd.army.mil.

FOR THE COMMANDER:

Encl

  
PHYLLIS M. RINEHART  
Deputy Chief of Staff for  
Information Management

ADB218773	ADB229914
ADB223531	ADB229497
ADB230017	ADB230947
ADB223528	ADB282209
ADB231930	ADB270846
ADB226038	ADB282266
ADB224296	ADB262442
ADB228898	ADB256670
ADB216077	
ADB218568	
ADB216713	
ADB216627	
ADB215717	
ADB218709	
ADB216942	
ADB216071	
ADB215736	
ADB216715	
ADB215485	
ADB215487	
ADB220304	
ADB215719	
ADB216072	
ADB222892	
ADB215914	
ADB222994	
ADB216066	
ADB217309	
ADB216726	
ADB216947	
ADB227451	
ADB229334	
ADB228982	
ADB227216	
ADB224877	
ADB224876	
ADB227768	
ADB228161	
ADB229442	
ADB230946	
ADB230047	
ADB225895	
ADB229467	
ADB224342	
ADB230950	
ADB227185	
ADB231856	